

Ultrastable, Highly Luminescent Organic–Inorganic Perovskite–Polymer Composite Films

Yanan Wang, Juan He, Hao Chen, Jiangshan Chen, Ruidong Zhu, Pin Ma, Andrew Towers, Yuan Lin, Andre J. Gesquiere, Shin-Tson Wu,* and Yajie Dong*

The past several years have witnessed the unprecedented efficiency up-rising of organic–inorganic perovskites (OIPs) based solar photovoltaics.^[1–3] Most recently, OIPs also emerged as promising light emitting materials with high efficiency and superb color purity.^[4,5] Despite the astonishing progress, instability under external stress remains one of the biggest challenges to overcome before OIPs can fulfill their promise as low cost, high performance photovoltaic or light emitting materials.^[6–8] Here we report a simple yet general strategy to achieve a series of ultrastable, highly luminescent $\text{CH}_3\text{NH}_3\text{PbBr}_3$ (MAPbBr₃) OIP–polymer composite films. Through a swelling–deswelling microencapsulation process, great dispersion and intimate passivation of crystalline OIP nanoparticles within polymer matrix have been achieved. This process yields composite films with high photoluminescence quantum yield (PLQY) of up to 48%, high color purity showing full width at half maxima (FWHM) down to 18 nm, and long average fluorescence lifetime (τ_{avg}) up to ≈ 502 ns. The OIP–polymer composite films possess unprecedented water and heat stability. MAPbBr₃–polystyrene

and MAPbBr₃–polycarbonate composite films without any additional barrier layers can survive boiling water treatment for 30 min with decay in PLQY of less than 15% and 7% respectively. Using these green emissive MAPbBr₃–polymer composite films and red CdSe-based quantum dots (QD)–polymer films as down-converters for blue light emitting devices (LEDs), we further demonstrated a white-light with record-high 95% color gamut in Rec. 2020, the new color standard for ultra-high definition TVs. We anticipate this strategy would enable OIPs to have widespread applications as backlight down converters for liquid crystal displays (LCDs), and it could lead to solution processed highly stable, vivid color light emitting devices, lasers or even high efficiency solar photovoltaics.

The instabilities of OIPs are often attributed to their low formation energy (≈ 0.1 – 0.3 eV), which makes it easy for them to be conveniently solution processed, but also renders them vulnerable to external stresses, such as moisture, heat, light, or electric field.^[6–8] It has been observed that, in the presence of moisture and oxygen, the OIP grains grow spontaneously even at room temperature, leading to a higher density of defects and a shorter carrier lifetime.^[9] Three passivation strategies have been developed to stabilize OIPs, but only with limited success. One commonly used approach involves film formation through impregnation and pore filling of a pre-formed mesoporous inorganic matrix (such as TiO_2 ^[10] or Al_2O_3 ^[11]) with the perovskite precursor solutions. However, the solvent evaporation from pre-formed, thus static, inorganic porous structures will inevitably lead to partially exposed, unprotected OIPs. In fact, it was reported that significant decomposition already occurs during annealing of OIPs on porous TiO_2 at 85 °C even in inert atmosphere.^[12] Further coverage of these OIP films with carbon nanotube/polymer composite demonstrated impressive “water resistant” devices,^[13] but such macroscale passivation leaves OIPs vulnerable to potential degradation due to film leakage. The second strategy, solution based synthesis of surfactant-protected OIP nanoparticles, can achieve passivation of individual nanocrystal grains and lead to colloidal OIPs with enhanced stability and PLQY.^[14–16] However, the reaction yield of OIP nanoparticles remains low and when the nanoparticles are processed as thin films, their efficiency tends to be substantially reduced because of quenching induced by spontaneous particle aggregations.^[17] The third strategy involves deposition of composite films from mixtures of OIP precursors with protecting media, such as organic small molecules, polymers^[18] or inorganic nanoparticles.^[19] Although inherently simple, this approach often results in serious phase separation between OIPs and the protecting media, leading to large OIP grain size variation, broad photoluminescence (PL) peaks, lower PLQY and unsatisfactory protection.

Y. N. Wang, H. Chen, Prof. J. S. Chen, A. Towers,
Prof. A. J. Gesquiere, Prof. Y. J. Dong
NanoScience Technology Center
University of Central Florida
Orlando, FL 32826, USA
E-mail: Yajie.Dong@ucf.edu

Y. N. Wang, P. Ma, Prof. Y. Lin
Beijing National Laboratory for Molecular Sciences
Key Laboratory of Photochemistry
Institute of Chemistry
Chinese Academy of Sciences
Beijing 100190, China

J. He, H. Chen, R. D. Zhu, Prof. A. J. Gesquiere,
Prof. S.-T. Wu, Prof. Y. J. Dong
College of Optics and Photonics
University of Central Florida
Orlando, FL 32816, USA
E-mail: swu@creol.ucf.edu

Prof. J. S. Chen
State Key Laboratory of Polymer Physics and Chemistry
Changchun Institute of Applied Chemistry
Chinese Academy of Sciences
Changchun 130022, China

A. Towers, Prof. A. J. Gesquiere
Department of Chemistry
University of Central Florida
Orlando, FL 32816, USA

Prof. A. J. Gesquiere, Prof. Y. J. Dong
Department of Materials Science and Engineering
University of Central Florida
Orlando, FL 32816, USA



DOI: 10.1002/adma.201603964

Here, we report a swelling–deswelling microencapsulation strategy to achieve well dispersed, intimately passivated OIP nanoparticles inside polymer matrixes and show that as-obtained OIP–polymer composite films have high photoluminescence efficiency, color purity and ultrahigh stability against heat and water exposure.

When being brought into contact with good solvents, polymer chains will swell and expand, letting in solvents and solutes. Such expansion is generally reversible through a deswelling process when solvent is evaporated.^[20] Dynamic polymer swelling–deswelling processes have been utilized in drug delivery to

introduce bioactive drugs into polymer matrixes as solutes and enable successful encapsulation and controlled release of the drugs.^[21] We hypothesize that OIP precursors can be introduced into polymer matrixes as solute through the solvent-induced polymer swelling process. When the solvent is driven out of the polymer matrix (for example, by baking), the OIP precursors will be left within to react and form high quality, well dispersed OIP nanoparticles. Meanwhile the polymer matrix will deswell, shrink back, and form a coherent barrier layer around the OIP nanoparticles, protecting them from water, oxygen, or heat of the surrounding environment (Figure 1a).

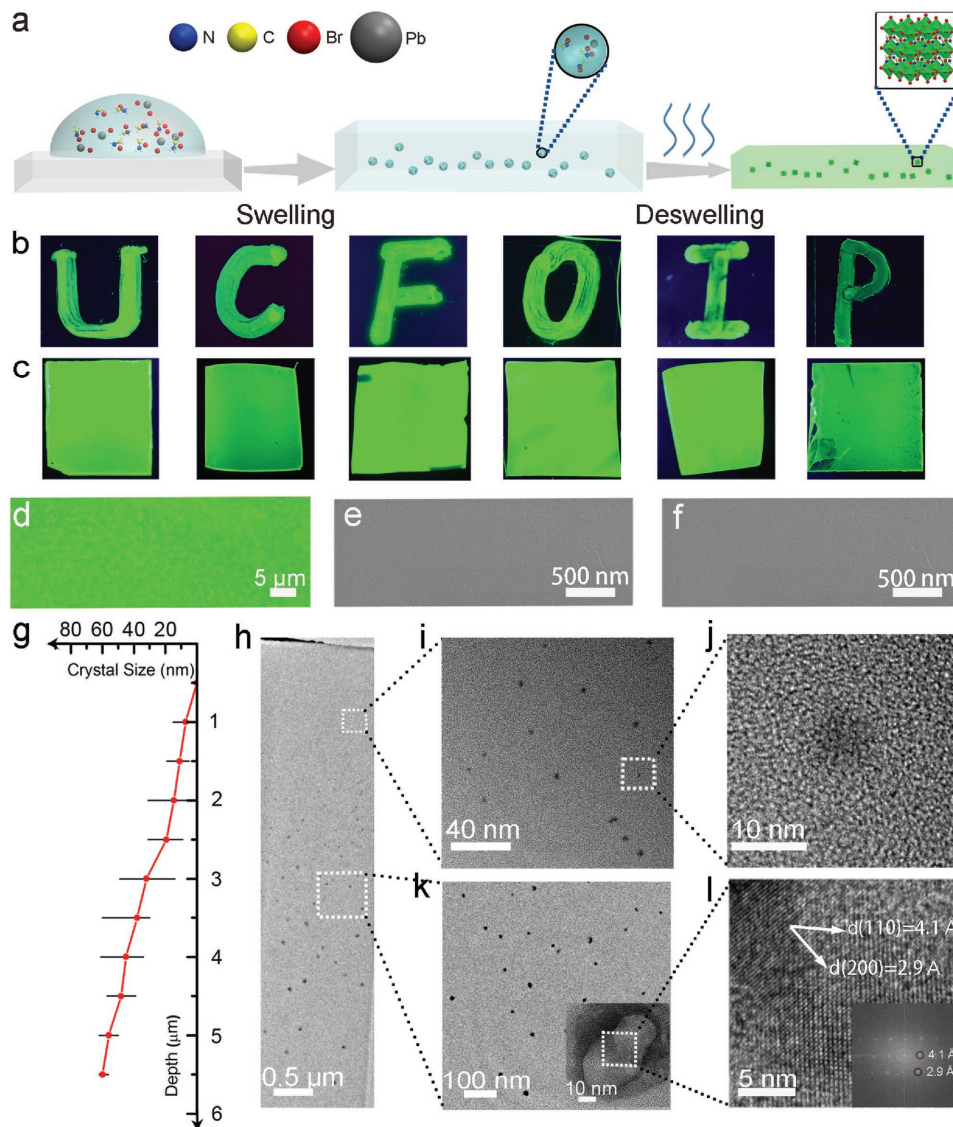


Figure 1. Swelling–deswelling microencapsulation strategy to OIP–polymer composite films. a) Scheme of MAPbBr₃–polymer composite film formation process through swelling–deswelling. Images of the luminescent composite samples prepared by b) cotton swab painting or c) spin coating under UV excitation (365 nm). Samples from left to right are MAPbBr₃–PS, MAPbBr₃–PC, MAPbBr₃–ABS, MAPbBr₃–CA, MAPbBr₃–PVC, and MAPbBr₃–PMMA respectively. d) Fluorescent optical microscope image of MAPbBr₃–PS film with focal plane ≈4 μm underneath the top surface. SEM images of PS surface e) before and f) after MAPbBr₃ spin coating and substrate annealing processing. g) Maximum, minimum and average size distribution of OIP crystal along with depth from top surface. h) Cross-section TEM image of MAPbBr₃–PS films showing the depth-dependent size-varied MAPbBr₃ nanoparticles embedded in PS. TEM image of highlighted area as in h, showing the well dispersed MAPbBr₃ nanoparticles at i) 1 μm and k) 3.5 μm depth respectively, Inset of (k) HRTEM image of single MAPbBr₃ nanoparticle. j) HRTEM image of highlighted area as in (i). l) HRTEM image of highlighted area as in (k), Inset: fast FFT of (l). All samples were prepared with precursor concentration of 5 mg mL⁻¹.

To demonstrate the principle, MAPbBr₃ OIP precursor solutions were prepared by mixing PbBr₂ and CH₃NH₃Br at a 1:3 molar ratio into dimethylformamide (DMF) solvent.^[18,19] A series of technically important polymer substrates, including polystyrene (PS), polycarbonate (PC), acrylonitrile butadiene styrene (ABS), cellulose acetate (CA), polyvinyl chloride (PVC), and poly(methyl methacrylate) (PMMA) which are known to swell in DMF, were tested to illustrate the generality of this strategy. Swelling happened once the precursor solutions were brought into contact with polymer substrates, either through simple cotton swab painting or spin-coating in a more controllable manner. Upon subsequent annealing of the substrates, visible color changes from transparent (for most polymers) or semiclear (for ABS film) to light green can be observed, indicating OIP phase formations along with solvent evaporation and polymer deswelling.

The fabrication process has been found to be robust and can tolerate variation of conditions (such as spin-coating speed or annealing temperature and time) to a certain degree (see Experimental Section). All MAPbBr₃-polymer composite films, obtained either with cotton swab painting (Figure 1b) or spin coating (Figure 1c), are luminescent under UV excitation. The most important technical aspect that affects the PLQY of as-prepared films is the overall precursor concentration. Along with the decreasing of precursor concentration, a systematic enhancement of PLQY has been observed (Table S1, Supporting Information), which could be due to reduced concentration quenching.^[22] Overall precursor concentration of 5 mg mL⁻¹ yields peak PLQY for all tested polymer substrates. Significantly, a record PLQY of ≈48% has been obtained for MAPbBr₃-ABS composite films, which is one of the highest values reported for MAPbBr₃ solid composite films to the best of our knowledge.^[4,19]

Microscopic characterizations of as-obtained MAPbBr₃-PS films provided direct proof for the swelling-deswelling microencapsulation hypothesis. When adjusting the focal plane of fluorescence microscopy to ≈4 μm underneath the top surface of the MAPbBr₃-PS sample, uniformly distributed nanoparticles over large area can be observed (Figure 1d), while focusing on the top surface yields no particle-like features. Scanning electron microscopy (SEM) characterization of the PS sample surfaces before (Figure 1e) and after (Figure 1f) MAPbBr₃ processing show identically smooth morphology with no visible OIP crystals on top, confirming that the nanocrystals observed in fluorescence microscopy are mainly embedded inside the polymer matrix and the substrate surface itself has fully recovered through the deswelling process. Similar embedded nanoparticles were also observed for MAPbBr₃-PC, MAPbBr₃-CA and MAPbBr₃-PVC composite films (Figures S1 and S2, Supporting Information). For semiclear MAPbBr₃-ABS, no particle-like features can be observed in fluorescence microscopy (Figure S1b, Supporting Information), probably due to the highly scattering nature of ABS polymers, but SEM indicates the originally rough ABS surface has been smoothed out after the spin coating process (Figure S2c,d, Supporting Information). For MAPbBr₃-PMMA, nanoparticles can be observed on the surface in both fluorescence microscopy and SEM images, probably due to relatively low swelling ratio of PMMA in DMF solvent.

Cross-sectional transmission electron microscopy (TEM) images (Figure 1g-l) of the MAPbBr₃-PS sample shows well dispersed crystalline nanoparticles intimately passivated within the amorphous PS substrate matrix. The nanoparticles show clear embedding-depth-dependence of size and density (Figure 1 g,h). Starting from <10 nm at ≈1 μm (Figure 1i,j) underneath the top surface, the sizes of nanoparticles gradually increase to >60 nm at ≈5–6 μm depth, along with particle density decreasing. From the high-resolution transmission electron microscopy (HRTEM) image (Figure 1l) and the fast Fourier transformation (FFT) image (inset of Figure 1l), interplanar distances of 2.9 and 4.1 Å corresponding to the (200) and (110) crystal faces of the MAPbBr₃ crystal can be identified. The energy-dispersive spectroscopy measurement shows that the nanoparticle has a Br/Pb molar ratio of 2.8:1 (Figure S3, Supporting Information), in accordance with the stoichiometry of MAPbBr₃. Clearly, MAPbBr₃ crystallization and nanocrystal dispersion in passivating polymer matrix have occurred simultaneously in the spin-coating, baking assisted swelling-deswelling process.

Figure 2 shows the static and transient PL behavior and absorption spectra of the spin-coated MAPbBr₃-polymer composite films. The abrupt absorption onsets and emission peaks in the 528–533 nm range correspond well with the band-to-band transition of bromide perovskite. Their FWHM range between 18 and 24 nm. This is comparable to previous colloidal MAPbBr₃ nanoparticles solution results^[15] and much narrower than what has been achieved with the MAPbBr₃-polymer precursor mixture approach (>30 nm) so far,^[18] indicating better color purity. Notably, such narrow emission peaks have been achieved with large variations of particle size and density (Figure 1g-l), implying size insensitivity of spectral width which is quite different from conventional inorganic quantum dots and could be due to that the intrinsic crystal structure of perovskite is similar to multiple quantum wells.^[23] It should be mentioned that along with precursor concentration increasing from 2 to 50 mg mL⁻¹, the peak wavelength showed consistent red shift (Figure S4 and Table S2, Supporting Information), which agrees with what was reported in mixed precursor approach.^[18] yet with narrower FWHM (Table S3, Supporting Information).

PL lifetimes are commonly taken as a hallmark of perovskite film quality, with longer decay lifetimes used as indicators of better performing materials^[24] For MAPbBr₃ based solid films^[19] or even colloidal nanoparticles,^[15] the average PL lifetimes (τ_{avg}) are usually within 10–100 ns. Remarkably, most MAPbBr₃-polymer composite films in this work showed long τ_{avg} ranging from 130 ns (for MAPbBr₃-PS) to 502 ns (for MAPbBr₃-ABS), with the only exception: the MAPbBr₃-PMMA sample with a τ_{avg} of ≈15 ns, which has the MAPbBr₃ nanoparticles on surface (Table S4, Supporting Information).

As results of good nanoparticle dispersion and polymer passivation, most MAPbBr₃-polymer composite films exhibit unprecedented stability against water and heat exposure. No observable PL degradation happened for most MAPbBr₃-polymer composite films upon exposure to ambient air for five months, except MAPbBr₃-PMMA, which degraded within an hour. To accelerate the test of water/moisture stability, the samples were put directly into water with their PL monitored periodically under

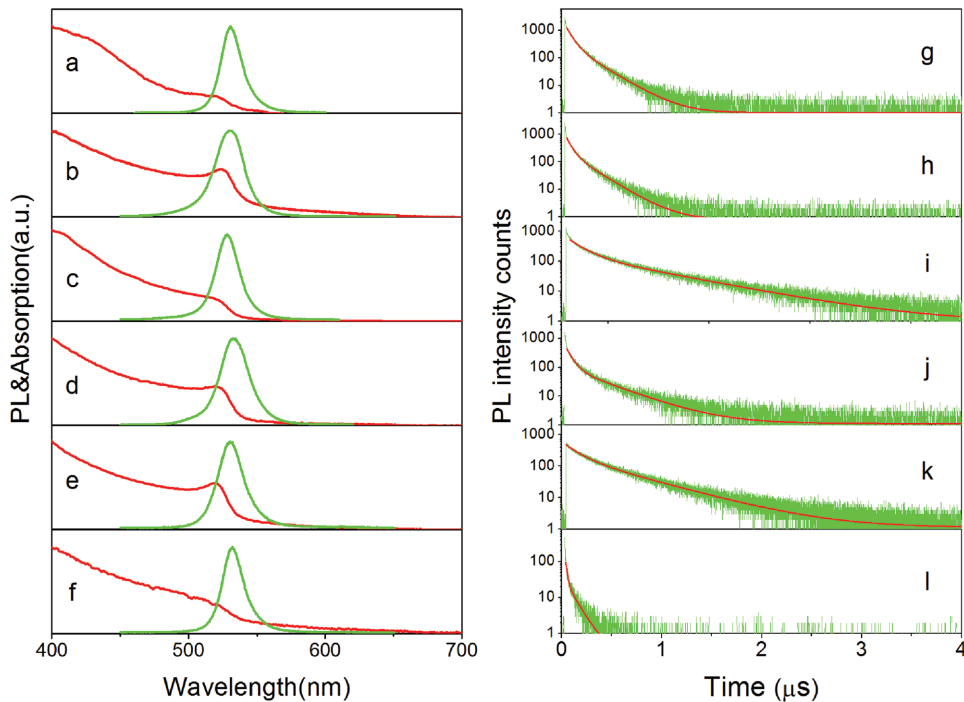


Figure 2. Optical properties of MAPbBr₃-polymer composite films. a–f) UV-vis absorption (red) and PL emission (green) spectra. g–l) PL decay (green) and fitting curves (red) for excitation at 467 nm and emission at ≈530 nm of various MAPbBr₃-polymer composite films. The samples from top to bottom are a,g) MAPbBr₃-PS, b,h) MAPbBr₃-PC, c,i) MAPbBr₃-ABS, d,j) MAPbBr₃-CA, e,k) MAPbBr₃-PVC, and f,l) MAPbBr₃-PMMA. All samples were prepared with precursor concentration of 5 mg mL⁻¹.

UV illumination (Figure 3a). The MAPbBr₃-PS, MAPbBr₃-PC, MAPbBr₃-PVC, and MAPbBr₃-ABS films immersed in water for two months reveal less than 7% decay in PLQY, indicating predominant water stability (Table S4, Supporting Information). As for MAPbBr₃-CA film, the brightness decayed to 5% of initial value after 48 h, probably because of the relatively higher water permeability of CA,^[25] while MAPbBr₃-PMMA became non-luminescent right after being put into water since the MAPbBr₃ crystals on surface were washed out right away.

The thermal stability of water stable MAPbBr₃-polymer composite films was then tested by heating up to high temperature and cooling back to room temperature while monitoring the PL spectra. Remarkably, the PL intensities (Figure 3), FWHM and peak wavelength (Figure S5, Supporting Information) of MAPbBr₃-PS and MAPbBr₃-PC can fully recover after being heated to 100 and 110 °C, respectively. Even after heating to 180 °C, the MAPbBr₃-PC still retains ≈40% of initial intensity when getting back to room temperature, indicating high thermal stability of these composite films even without any special barrier layer protection. As for MAPbBr₃-ABS film, the decrease of perovskite brightness after cooling back from 100 °C might come from the degradation of ABS substrate, the rubbery phase of which is known to be susceptible to environmental degradation at higher temperature.^[26] It is noted that for all three samples, no obvious changes were observed in the UV-vis absorption peaks and onsets after heating, indicating intact MAPbBr₃ nanocrystals (Figure S6, Supporting Information).

Furthermore, The MAPbBr₃-PS and MAPbBr₃-PC samples were heated up to different temperatures and held for extended

period of time to test their long-time high temperature stability (Figure S7, Supporting Information). It is observed that even at 100 °C which is around PS's glass transition temperature (T_g), the sample can maintain more than 65% of initial brightness after continuous heating for ≈5 h. For MAPbBr₃-PC films ($T_g = 147$ °C) tested at 110 or 140 °C, surprisingly, significant brightness enhancements were observed for the first hour, which could be attributed to photoenhancement, a behavior that has been reported for traditional quantum dots^[27] or perovskite,^[28] often at room temperature. Impressively, continuous test for ≈10 h at these temperatures did not lead to obvious decay for MAPbBr₃-PC films. Tests at 180 °C, which is much higher than T_g of PC, led to quick luminescence decay, indicating that thermal stability of the perovskite-polymer composite films are mainly limited by the thermal stability of polymer substrates.

The temperature dependent PL data within the reversible temperature range (Figure 3b,c) can be fitted using Equation (1)^[29]

$$I(T) = \frac{I_0}{1 + Ae^{-E_b/k_B T}} \quad (1)$$

in which I_0 is the intensity at 0 K, k_B is the Boltzmann constant and E_b is the binding energy. For MAPbBr₃-PS we get $E_b = 270 \pm 15$ meV and for MAPbBr₃-PC $E_b = 322 \pm 12.5$ meV (Figure 3b,c). This is approaching the value of colloidal OIP nanoparticles in solution and over four times larger than the bulk MAPbBr₃ value (50–70 meV).^[15] Such a large binding energy implies a higher possibility of trapping in radiative state rather than escaping and recombining non-radiatively,

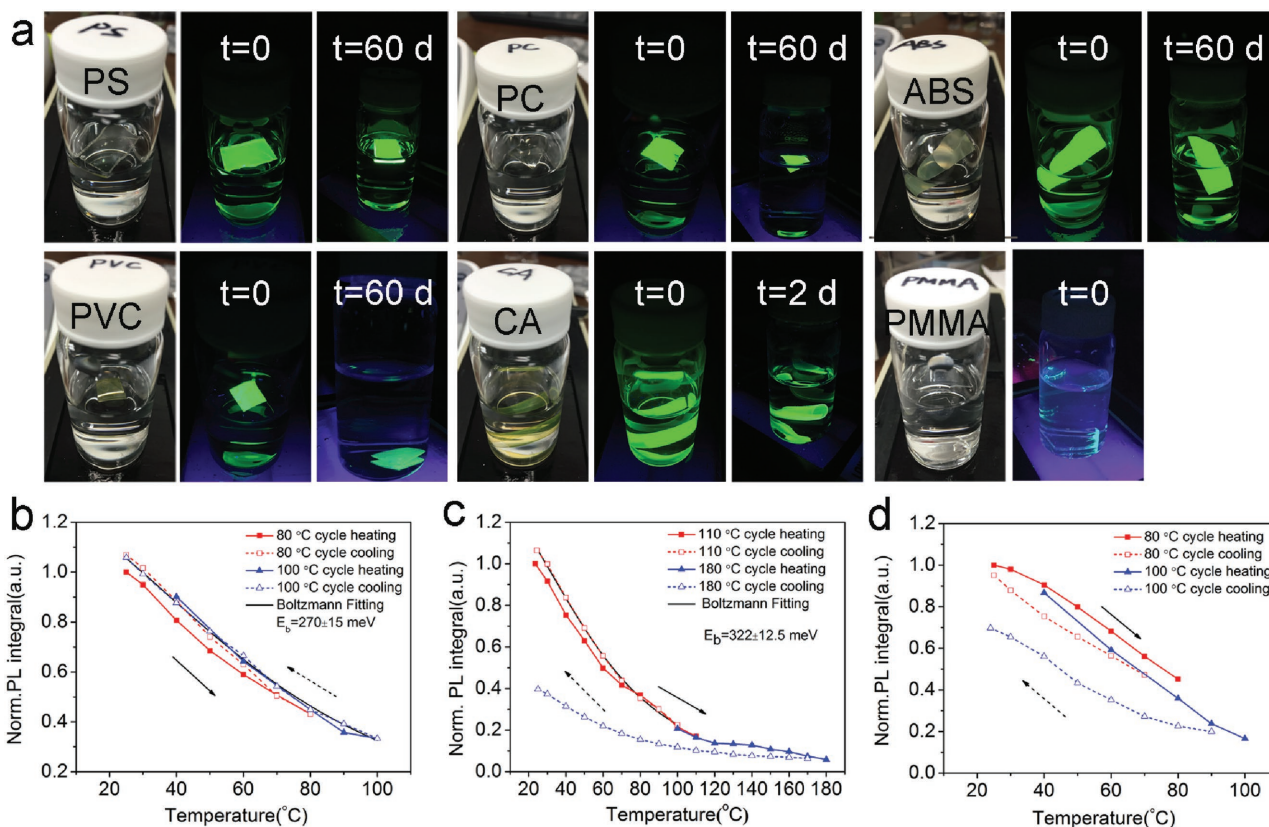


Figure 3. Water and thermal stability characterizations. a) Photographs taken under white light or UV irradiation at indicated time period. The composite film samples immersed in water are MAPbBr₃-PS, MAPbBr₃-PC, MAPbBr₃-ABS, MAPbBr₃-PVC, MAPbBr₃-CA, and MAPbBr₃-PMMA. Temperature-dependent PL intensity of b) MAPbBr₃-PS, c) MAPbBr₃-PC, and d) MAPbBr₃-ABS. Squares mark the first thermal cycle and triangles represent the second thermal cycle. The solid symbols refer to heating stages and open symbols to cooling stages. Black lines in (b,c) indicate Boltzmann fittings for the reversible heating, cooling processes.

so the PL emission is more likely to originate from the exciton recombination rather than the recombination from free electrons and holes.^[30] The high exciton binding energy could benefit from good nanoparticle dispersion and surface passivation by surrounding polymer chains.

Selected from their good water and thermal stability, MAPbBr₃-PS and MAPbBr₃-PC films were then tested in harsh environment: boiling water. It has been observed that these OIP-polymer composite films remain highly luminescent both in and after removal from boiling water (Videos S1 and S2, Supporting Information), and the remained morphology, brightness, and structure are confirmed by microscopic, PL, and absorption characterizations before and after boiling (Figure S8, Supporting Information). PLQY characterizations after boiling the samples for 30 min showed decay of only less than 7% for MAPbBr₃-PC and 15% for MAPbBr₃-PS films (Table S5, Supporting Information). In comparison, the luminescence of MAPbBr₃ films encapsulated with macroscopic PS or PC films^[13] were completely lost within 10 s in boiling water and cannot be recovered (Videos S3 and S4, Supporting Information).

Because of their process simplicity, low cost, high stability, high luminescence efficiency, and color purity, these OIP-polymer composite films have great potential for various

applications. The most immediate usage would be as down-converters for the backlight unit (BLU) of LCDs.^[31] For concept demonstration, a green MAPbBr₃-PS film and a red CdSe based QD-polymer film were prepared. Under UV light, these films emit bright and pure red or green lights (Figure 4a). We applied the “remote-phosphor” approach by using a high power (550 mW) blue LED (450 nm with a FWHM of 20 nm) to pump the green perovskite-polymer composite film and the red QD film. The resultant red (630 nm with a FWHM of 23 nm) and green (532 nm with a FWHM of 18 nm) spectra can be well fitted by the Gaussian function. Overall the system can cover over 100% of the Adobe RGB color gamut and 95% of the Rec. 2020 color gamut, the white point is D65, as is illustrated in Figure 4d. A similar approach has recently been commercialized by 3M/Nanosys and QD Vision^[32] with green and red QDs. Compared with the all-QD approach that uses green QDs with FWHM of ≈30 nm, our hybrid film has the advantage that the green perovskite emission has narrower linewidth (18 nm), indicating more pure green color, which is vital for wider color gamut.

The above studies illustrate a simple swelling-deswelling microencapsulation strategy to overcome the major instability challenge for OIP materials. The demonstrated stability, high efficiency, and high color purity of the green OIP-composite

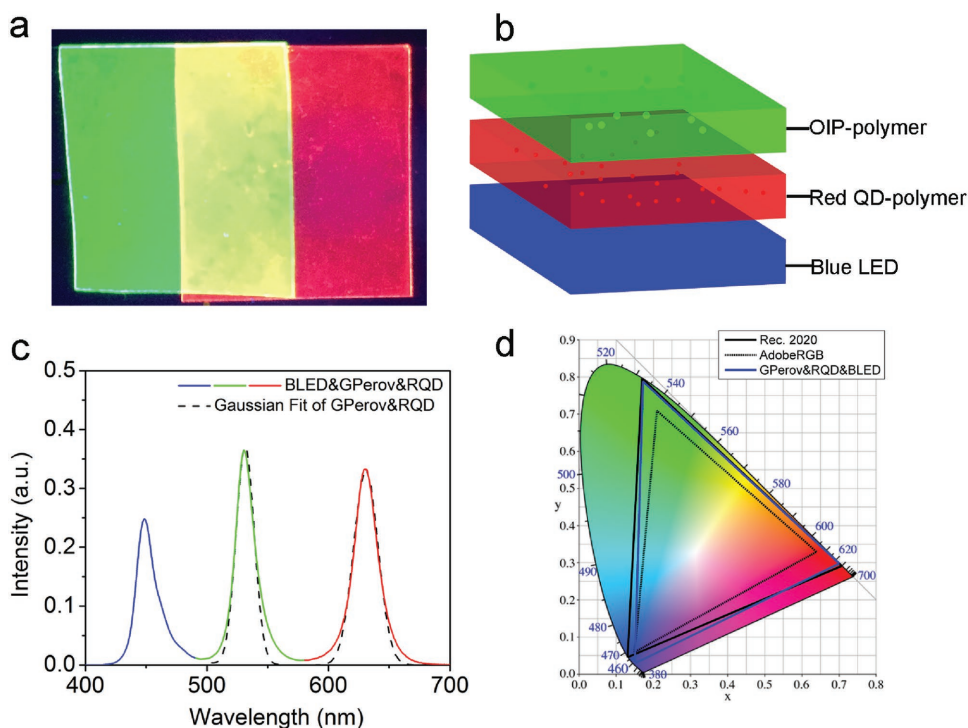


Figure 4. Application of MAPbBr₃-Polymer composite films as down converters for back light units of wide color gamut displays. a) Photograph of red QD-PS and MAPbBr₃-PS composite films under UV illumination. b) Scheme of white light generation by integrating red QD-PS and MAPbBr₃-PS films with blue light emitting diodes. c) Emission spectra of a white LED system with green MAPbBr₃-PS and red QD-PS films as down converters for blue LEDs. Dashed lines refer to Gaussian fit for green and red emission spectra. d) Color gamut coverage of the white LED systems (blue) with adobe RGB (gray) and Rec. 2020 (black) standards for comparison in CIE 1931.

materials bodes well for their near term applications in LCD BLU down converters. Because of the generality of swelling-deswelling process in polymers, we believe this strategy will be applicable to other OIPs (e.g., MAPbI₃), solvents and polymers systems, enabling other highly stable OIP-polymer composite films. Provided that electrical transport properties of such components can be further enhanced (e.g., by doping with conductive nanoparticles), such components could become critical elements for highly stable light emitting devices,^[33] lasers,^[34] or even solar photovoltaics.

Experimental Section

Materials: Polycarbonate films, acrylonitrile-butadiene-styrene films, cellulose acetate films, polyvinyl chloride films, and polymethylmethacrylate sheets were purchased from McMaster-Carr. Polystyrene substrates were purchased from VWR International, Inc. CH₃NH₃Br (CH₃NH₃ = MA) was purchased from Luminescence Technology Corp. PbBr₂ (99%) and *N,N*-dimethylformamide (extra dry, 99%) were purchased from Sigma-Aldrich. Unless stated otherwise, all materials were used as received.

Synthesis: Perovskite-polymer composite films, MABr and PbBr₂ (3:1 molar ratio) with overall concentration of 100 mg mL⁻¹ were prepared in DMF while stirring for overnight before use. The solution was further diluted in DMF to give a different concentration of 2, 5, 10, 20, 50 mg mL⁻¹. MAPbBr₃ solutions were processed onto different polymer film substrates through cotton swab painting or spin-coating at 2000–4000 rpm, followed by baking at 30–80 °C for 2–8 h inside a glovebox.

Perovskite on Glass Control Sample Preparation: MABr and PbBr₂ (3:1 molar ratio) with overall concentration of 100 mg mL⁻¹ in DMF were spin coated on the glass at 3000 rpm and dried at room temperature overnight inside glovebox. PS and PC were dissolved in chloroform at a concentration 100 mg mL⁻¹. The polymer solutions were deposited on top of the perovskite layer by spin-coating at 3000 rpm and baked at 60 °C for 30 min. No obvious change in brightness under UV irradiation was observed after coating the polymer layer.

CdSe based red quantum dots were synthesized following reported methods.^[35] Quantum dots in chlorobenzene were spin coated at 3000 rpm on a PS film to obtain the red luminescent film.

Characterizations: Fluorescence images were taken using an Olympus BX51 microscope. Light source of 450–480 nm was used for excitation. Scanning electron microscope characterizations were carried out with a high resolution field-emission SEM (Philips-FEI XL30-SFEG). All samples for SEM measurements were coated with Au. TEM analyses on the cross-sections of the MAPbBr₃-polymer composite films were carried out using FEI Tecnai F30 TEM. The cross-sectional samples were prepared using FEI 200 TEM focused-ion-beam instrument.

The PLQY of the films was measured by the integrating sphere method at Changchun Institute of Applied Chemistry, China. An intensity-modulated 409 nm laser beam was used for excitation. The blank sample of each polymer substrate was firstly measured, and the absorption effect of the polymer films was deducted when calculating the PLQY. All the PLQY measurements were carried out in air at room temperature.

UV-vis absorption spectra were recorded on a CARY 300 Bio spectrophotometer at room temperature. The steady-state PL of MAPbBr₃-polymer films was measured using Horiba Nanolog Spectrofluorometer.

With a home-built sample-scanning confocal microscope described elsewhere,^[36] Time correlated single photon counting (TCSPC) excited

state lifetime studies were completed by parking an area of interest of the samples over the focused pulsed laser beam (Picoquant LDH-P-C-470), and collecting photons with a fast single photon counting detector (Picoquant, Micro Photon Devices, PDM series). Photon timing was measured using a pulsed laser driver (PDL 800-D) that provided the timing signal to a PicoHarp 300 TCSPC module in combination with a detector router (PHR 800), all from Picoquant.

The time-resolved PL decay curves were fitted with a biexponential function of time (t)

$$F(t) = f_1 e^{-t/\tau_1} + f_2 e^{-t/\tau_2} \quad (2)$$

where f_1 and f_2 are prefactors, τ_1 and τ_2 are the time constants. The average recombination lifetime (τ_{ave}) is estimated with the f and τ values from the fitted curve data according to the following equation

$$\tau_{\text{avg}} = f_1 \tau_1 + f_2 \tau_2 \quad (3)$$

Stability Tests: For water stability test, all MAPbBr₃-polymer composite films without further protection were immersed in de-ion water at room temperature for two months.

For temperature-dependent PL measurements, the samples were put inside the Linkam LTS350 cryostat, with a heating rate of 5 °C min⁻¹. The temperature tunable range was up to 350 °C. Laser excitation at 457 nm (Argon laser: Stellar-Pro Select 150) was used and the MAPbBr₃-polymer films were in situ heated on the stage whose temperature was controlled by a temperature controller (Linkam TMS 94). The composite films were heated up to a certain temperature, held for 2–3 min to be stable, measured for the spectra (Ocean Optics Spectrometer USB 2000+) and then proceeded to the next temperature point immediately.

For long term thermal stability test, MAPbBr₃-PC was heated directly up to 110, 140 °C (close to PC's glass transition temperature 147 °C) or 180 °C, and MAPbBr₃-PS was heated up to 100 °C (≈glass transition temperature of PS) and then kept at that temperature for a certain period (≈ 5–10 h) to see the trend of PL integrated intensity.

For boiling water test, MAPbBr₃-PS and MAPbBr₃-PC composite films were put into boiling water for 10 s, 10 min, and 30 min subsequently before they were taken out, and cooled down to room temperature for optical microscope, UV-vis absorption spectra, and PLQY characterizations.

For "remote phosphor" white light generation, a 550 mW high power blue (450 nm) LED (Royal-Blue Cree XLamp XT-E from LEDsupply) was used to excite the green perovskite-polymer composite film and the red QD-polymer film.

During revision of the manuscript, a report of "In Situ Fabrication of Halide Perovskite Nanocrystal-Embedded Polymer Composite Films with Enhanced Photoluminescence for Display Backlights" came to the authors' attention,^[37] which represents new progress of the mixed precursor approach.^[18] with improved photoluminescence spectra purity, better water stability, yet still limited thermal stability.

Supporting Information

Supporting Information is available from the Wiley Online Library or from the author.

Acknowledgements

Y.W., J.H., and H.C. contributed equally to this work. The authors thank J. Thomas, C. Li, and L. Tetard for helpful discussion and the Materials Characterization Facility (MCF), University of Central Florida for HRTEM characterization. Y. Dong is grateful for support of this work by University of Central Florida through a startup funding (Grant No. 20080738) and an in-house grant (Grant No. 63019028). S. Wu acknowledges partial support of AFOSR under contract No. FA9550-14-1-0279. A. J. Gesquiere

thanks the National Science Foundation (NSF) for financial support of this work through award CMMI-1335295. Y. Lin acknowledges support of the National Natural Science Foundation of China (Grant No. 51303186) and 973 National Research Fund for Fundamental Key Project (2012CB932903).

Received: July 26, 2016

Revised: September 8, 2016

Published online: October 17, 2016

- [1] a) J. Berry, T. Buonassisi, D. A. Egger, G. Hodes, L. Kronik, Y. L. Loo, I. Lubomirsky, S. R. Marder, Y. Mastai, J. S. Miller, D. B. Mitzi, Y. Pas, A. M. Rappe, I. Riess, B. Rybtchinski, O. Stafsudd, V. Stevanovic, M. F. Toney, D. Zitoun, A. Kahn, D. Ginley, D. Cahen, *Adv. Mater.* **2015**, *27*, 5102; b) H. J. Snaith, *J. Phys. Chem. Lett.* **2013**, *4*, 3623; c) M. A. Green, A. Ho-Baillie, H. J. Snaith, *Nat. Photonics* **2014**, *8*, 506.
- [2] a) A. Kojima, K. Teshima, Y. Shirai, T. Miyasaka, *J. Am. Chem. Soc.* **2009**, *131*, 6050; b) M. Lee, J. Teuscher, T. Miyasaka, T. Murakami, H. J. Snaith, *Science* **2012**, *338*, 643; c) M. Liu, M. B. Johnston, H. J. Snaith, *Nature* **2013**, *501*, 395; d) J. Burschka, N. Pellet, S. J. Moon, R. Humphry-Baker, P. Gao, M. K. Nazeeruddin, M. Grätzel, *Nature* **2013**, *499*, 316.
- [3] a) H. Zhou, Q. Chen, G. Li, S. Luo, T.-b. Song, H.-S. Duan, Z. Hong, J. You, Y. Liu, Y. Yang, *Science* **2014**, *345*, 542; b) N. J. Jeon, J. H. Noh, Y. C. Kim, W. S. Yang, S. Ryu, S. Seok, *Nat. Mater.* **2014**, *13*, 897; c) W. S. Yang, J. H. Noh, N. J. Jeon, Y. C. Kim, S. Ryu, J. Seo, S. I. Seok, *Science* **2015**, *348*, 1234; d) W. Y. Nie, H. Tsai, R. Asadpour, J. C. Blancon, A. J. Neukirch, G. Gupta, J. J. Crochet, M. Chhowalla, S. Tretiak, *Science* **2015**, *347*, 522; e) X. Li, D. Bi, C. Yi, J. D. Décoppet, J. Luo, S. M. Zakeeruddin, A. Hagfeldt, M. Grätzel, *Science* **2016**, *353*, 58.
- [4] a) S. D. Stranks, H. J. Snaith, *Nat. Nano* **2015**, *10*, 391; b) S. Gonzalez-Carrero, R. E. Galian, J. Perez-Prieto, *Opt. Express* **2016**, *24*, A285; c) Y. Zhao, K. Zhu, *Chem. Soc. Rev.* **2016**, *45*, 655; d) S. A. Veldhuis, P. P. Boix, N. Yantara, M. Li, T. C. Sum, N. Mathews, S. G. Mhaisalkar, *Adv. Mater.* **2016**, *28*, 6804.
- [5] a) S. Pathak, N. Sakai, F. Wisnivesky Rocca Rivarola, S. D. Stranks, J. Liu, G. E. Eperon, C. Ducati, K. Wojciechowski, J. T. Griffiths, A. A. Haghighirad, A. Pellaroque, R. H. Friend, H. J. Snaith, *Chem. Mater.* **2015**, *27*, 8066; b) F. Deschler, M. Price, S. Pathak, L. E. Klüntberg, D. D. Jarausch, R. Higler, S. Hüttner, T. Leijtens, S. D. Stranks, H. J. Snaith, M. Atature, R. T. Phillips, R. H. Friend, *J. Phys. Chem. Lett.* **2014**, *5*, 1421; c) Z. Ning, X. Gong, R. Comin, G. Walters, F. Fan, O. Voznyy, E. Yassitepe, A. Buin, S. Hoogland, E. H. Sargent, *Nature* **2015**, *523*, 324.
- [6] a) E. von Hauff, M. Lira-Cantu, T. M. Brown, H. Hoppe, *Adv. Energy Mater.* **2015**, *5*, 1501924; b) T. Leijtens, G. E. Eperon, N. K. Noel, S. N. Habisreutinger, A. Petrozza, H. J. Snaith, *Adv. Energy Mater.* **2015**, *5*, 1500963; c) L. Loo, P. Patel, *MRS Bull.* **2015**, *40*, 636.
- [7] G. Niu, X. Guo, L. Wang, *J. Mater. Chem. A* **2015**, *3*, 8970.
- [8] a) T. A. Berhe, W. N. Su, C. H. Chen, C. J. Pan, J. H. Cheng, H. M. Chen, M. C. Tsai, L. Y. Chen, A. A. Dubale, B. J. Hwang, *Energy Environ. Sci.* **2016**, *9*, 323; b) M. Shahbazi, H. Wang, *Solar Energy* **2016**, *123*, 74.
- [9] R. Sheng, X. Wen, S. Huang, X. Hao, S. Chen, Y. Jiang, X. Deng, M. Green, A. Ho-Baillie, *Nanoscale* **2016**, *8*, 1926.
- [10] T. Leijtens, B. Lauber, G. E. Eperon, S. D. Stranks, H. J. Snaith, *J. Phys. Chem. Lett.* **2014**, *5*, 1096.
- [11] S. Guarnera, A. Abate, W. Zhang, J. M. Foster, G. Richardson, A. Petrozza, H. J. Snaith, *J. Phys. Chem. Lett.* **2015**, *6*, 432.
- [12] B. Conings, J. Drijkoningen, N. Gauquelin, A. Babayigit, J. D'Haen, L. D'Olieslaeger, A. Ethirajan, J. Verbeeck, J. Manca, E. Mosconi, *Adv. Energy Mater.* **2015**, *5*, 1500477.

- [13] S. N. Habisreutinger, T. Leijtens, G. E. Eperon, S. D. Stranks, R. J. Nicholas, H. J. Snaith, *Nano Lett.* **2014**, *14*, 5561.
- [14] a) L. C. Schmidt, A. Pertegás, S. González-Carrero, O. Malinkiewicz, S. Agouram, G. Mínguez Espallargas, H. J. Bolink, R. E. Galian, J. Pérez-Prieto, *J. Am. Chem. Soc.* **2014**, *136*, 850; b) B. Luo, Y. Pu, Y. Yang, S. Lindley, G. Abdelmageed, H. Ashry, Y. Li, X. Li, J. Zhang, *J. Phys. Chem. C* **2015**, *119*, 26672; c) P. Tyagi, S. M. Arveson, W. A. Tisdale, *J. Phys. Chem. Lett.* **2015**, *6*, 1911; d) H. Huang, A. S. Susha, S. V. Kershaw, T. F. Hung, A. L. Rogach, *J. Adv. Sci.* **2015**, *2*, 1500194.
- [15] a) F. Zhang, H. Zhong, C. Chen, X.-G. Wu, X. Hu, H. Huang, J. Han, B. Zou, Y. Dong, *ACS Nano* **2015**, *9*, 4533; b) O. Vyborny, S. Yakunina, M. V. Kovalenko, *Nanoscale* **2016**, *8*, 6278.
- [16] L. Protesescu, S. Yakunina, M. I. Bodnarchuk, F. Krieg, R. Caputo, C. H. Hendon, R. X. Yang, A. Walsh, M. C. Kovalenko, *Nano Lett.* **2015**, *15*, 3692.
- [17] F. Zhu, L. Men, Y. Guo, Q. Zhu, U. Bhattacharjee, P. M. Goodwin, J. W. Petrich, E. A. Smith, J. Vela, *ACS Nano* **2015**, *9*, 2948.
- [18] D. Di, K. P. Musselman, G. Li, A. Sadhanala, Y. Ievskaya, Q. Song, Z.-K. Tan, M. L. Lai, J. L. MacManus-Driscoll, N. C. Greenham, R. H. Friend, *J. Phys. Chem. Lett.* **2015**, *6*, 446.
- [19] G. Longo, A. Pertegás, L. Martínez-Sarti, M. Sessolo, H. J. Bolink, *J. Mater. Chem. C* **2015**, *3*, 11286.
- [20] B. Erman, P. Flory, *Macromolecules* **1986**, *19*, 2342.
- [21] a) S. Freitas, H. P. Merkle, B. Gander, *J. Controlled Release* **2005**, *102*, 313; b) M. Li, O. Rouaud, D. Poncelet, *Int. J. Pharm.* **2008**, *363*, 26.
- [22] D. Dexter, J. H. Schulman, *J. Chem. Phys.* **1954**, *22*, 1063.
- [23] Y. H. Kim, H. Cho, J. H. Heo, T. S. Kim, N. Myoung, C. L. Lee, S. H. Im, T. W. Lee, *Adv. Mater.* **2015**, *27*, 1248.
- [24] D. W. deQuilettes, S. M. Vorpahl, S. D. Stranks, H. Nagaoka, G. E. Eperon, M. E. Ziffer, H. J. Snaith, D. S. Ginger, *Science* **2015**, *348*, 683.
- [25] L. W. McKeen, *Permeability Properties of Plastics and Elastomers*. William Andrew, Elsevier, Amsterdam, The Netherlands, **2011**.
- [26] N. Grassie, G. Scott, *Polymer Degradation and Stabilisation*. Cambridge University Press, Cambridge **1985**.
- [27] C. Carrillo-Carrión, S. Cárdenas, B. M. Simonet, M. Valcárcel, *Chem. Commun.* **2009**, 5214.
- [28] Y. Tian, A. Merdasa, E. Unger, M. Abdellah, K. Zheng, S. McKibbin, A. Mikkelsen, T. Pullerits, A. Yartsev, V. Sundström, I. G. Scheblykin, *J. Phys. Chem. Lett.* **2015**, *6*, 4171.
- [29] a) Z. Chen, C. Yu, K. Shum, J. J. Wang, W. Pfenninger, N. Vockic, J. Midgley, J. T. Kenney, *J. Lumin.* **2012**, *132*, 345; b) K. Wu, A. Bera, C. Ma, Y. M. Du, Y. Yang, L. Li, T. Wu, *Phys. Chem. Chem. Phys.* **2014**, *16*, 22476.
- [30] S. D. Stranks, V. M. Burlakov, T. Leijtens, J. M. Ball, A. Goriely, H. J. Snaith, *Phys. Rev. Appl.* **2014**, *2*, 034007.
- [31] a) Z. Luo, D. Xu, S.-T. Wu, *J. Display Technol.* **2014**, *10*, 526; b) R. Zhu, Z. Luo, H. Chen, Y. Dong, S.-T. Wu, *Opt. Express* **2015**, *23*, 23680.
- [32] a) J. Chen, S. Gensler, J. Hartlove, J. Yurek, E. Lee, J. Thielen, J. Van Derlofske, J. Hillis, G. Benoit, J. Tibbits, *SID Int. Symp. Dig. Tech. Pap.* **2015**, *46*, 173; b) J. S. Steckel, J. Ho, C. Hamilton, J. Xi, C. Breen, W. Liu, P. Allen, S. Coe-Sullivan, *J. Soc. Inf. Disp.* **2015**, *23*, 294.
- [33] a) Z.-K. Tan, R. S. Moghaddam, M. L. Lai, P. Docampo, R. Higler, F. Deschler, M. Price, A. Sadhanala, L. M. Pazos, D. Credgington, F. Hanusch, T. Bein, H. J. Snaith, R. H. Friend, *Nat. Nano* **2014**, *9*, 687; b) H. Cho, S.-H. Jeong, M.-H. Park, Y.-H. Kim, C. Wolf, C.-L. Lee, J. H. Heo, A. Sadhanala, N. Myoung, S. Yoo, *Science* **2015**, *350*, 1222.
- [34] a) G. Xing, N. Mathews, S. S. Lim, N. Yantara, X. Liu, D. Sabba, M. Grätzel, S. Mhaisalkar, T. C. Sum, *Nat. Mater.* **2014**, *13*, 476; b) S. W. Eaton, M. Lai, N. Gibson, A. B. Wong, L. Dou, J. Ma, L. Wang, S. R. Leone, P. Yang, *Proc. Natl. Acad. Sci. USA* **2016**, *113*, 1993; c) H. M. Zhu, Y. P. Fu, F. Meng, X. X. Wu, Z. Z. Gong, Q. Ding, M. V. Gustafsson, M. T. Trinh, S. Jin, X. Y. Zhu, *Nat. Mater.* **2015**, *14*, 636; d) Q. Zhang, S. T. Ha, X. F. Liu, T. C. Sum, Q. H. Xiong, *Nano Lett.* **2014**, *14*, 5995.
- [35] W. H. Liu, C. Breen, WO 2013/078245 A1, **2013**.
- [36] D. Tenery, J. G. Worden, Z. J. Hu, A. J. Gesquiere, *J. Lumin.* **2009**, *129*, 423.
- [37] Q. Zhou, Z. Bai, W. G. Lu, Y. Wang, B. Zou, H. Z. Zhong, *Adv. Mater.* **2016**, DOI: 10.1002/adma.201602651.